Journal of Power Sources 213 (2012) 249–254

Contents lists available at SciVerse ScienceDirect

Journal of Power Sources

journal homepage: www.elsevier.com/locate/jpowsour

Short communication

High gravimetric capacity and long cycle life in Mn_3O_4/graphene platelet/LiCMC composite lithium-ion battery anodes

Nathalie Lavoie, Patrick R.L. Malenfant [1], Fabrice M. Courtel, Yaser Abu-Lebdeh*, Isobel J. Davidson

National Research Council Canada, 1200 Montreal Road, Ottawa, Ontario, Canada K1A 0R6

ARTICLE INFO

Article history:
Received 19 January 2012
Received in revised form
19 March 2012
Accepted 21 March 2012
Available online 7 April 2012

Keywords:
Graphene
Manganese oxide
Li-ion batteries
Anode materials
Lithium carboxymethyl cellulose (LiCMC)

ABSTRACT

We report the synthesis, characterization and battery performance of a novel Mn_3O_4/graphene composite based on graphene platelets and also an Mn_3O_4/reduced-graphene-oxide composite for comparison. The electrodes were cast from aqueous dispersions in which lithium carboxymethyl cellulose was used as a binder thus enabling an aqueous based process for anode fabrication. The Mn_3O_4/graphene-platelet and the Mn_3O_4/reduced-graphene-oxide composites anode system possess high gravimetric capacities ($\sim$700 mAh g^{-1}) and excellent cycling stability (>100 cycles).

1. Introduction

Transition metal oxides (TMOs) such as Mn_3O_4 have been explored as anode materials to replace graphite in lithium-ion batteries due to their higher theoretical reversible capacities (937 mAh g^{-1}) [1–5]. However TMOs often suffer from pulverization due to volume change upon cycling thus leading to rapid capacity fade. Nevertheless, Mn_3O_4 is an attractive anode material for lithium-ion batteries because it is environmentally friendly, relatively low cost, and is one of the most abundant TMOs. Manganese is even more appealing when considering the low observed oxidation potential of manganese nanoparticles (1.2 V) [6] compared to other transition metals such as cobalt that exhibit an oxidation potential of about 2 V [1,7]. However Mn_3O_4 is limited by a low intrinsic electrical conductivity of 2×10^{-7} S cm^{-1}.[8] More recently graphene has been combined with TMOs in hopes of improving performance both in terms of gravimetric capacity and cycle life. Graphene can potentially serve as an excellent matrix due to its tunable surface area, mechanical flexibility and high electrical conductivity [9]. To date, several preliminary studies of metal oxide/graphene composite anode materials have been reported [10–14] but in many cases only short cycling [15–17] schedules have been demonstrated for these composite systems, thus precluding any definitive conclusions from being drawn regarding graphene's suitability as a component for anode materials in lithium-ion batteries.

Furthermore, reports describing TMO/graphene composites in lithium-ion batteries have so far been exclusively prepared from reduced graphene oxide (RGO). RGO is typically made using the Hummers method or via similar oxidative processes to yield graphene oxide (GO). Several methods can be applied to reduce GO, thus providing RGO with varying levels of chemical functionality [18–20]. These processes are resource intensive (e.g. large volumes of solvents/reagents are consumed) thus in the absence of the benefits of economies of scale and efficient recycling protocols, RGO is often considered prohibitively expensive. Alternatively, graphene platelets, which are nominally thinner than graphite but thicker than few layer RGO, present a compelling alternative due to their tunable properties (i.e. surface area and particle size), near defect-free surface and low cost. Their availability in large quantities and lower cost compared to RGO make graphene platelets an appealing candidate for the development of composite anode materials in lithium-ion batteries.

Herein, we report the synthesis and characterization of a novel Mn_3O_4/graphene composite material based on graphene platelets and we compare its performance to the RGO composite. Their performance as the active anode material in lithium-ion batteries

* Corresponding author. Tel.: +1 6139494184; fax: +1 6139900347.
E-mail addresses: Patrick.Malenfant@nrc-cnrc.gc.ca (P.R.L. Malenfant), Yaser.Abu-Lebdeh@nrc-cnrc.gc.ca (Y. Abu-Lebdeh).
[1] Tel.: +16139900705; fax: +16139912384.

0378-7753/$ – see front matter
doi:10.1016/j.jpowsour.2012.03.055

was assessed using lithium carboxymethyl cellulose (LiCMC) as the binder in lieu of the more conventional binder polyvinylidene fluoride (PVDF) due to the former's processability in water and superior performance in preliminary tests [6,21]. To the best of our knowledge graphene composite anodes fabricated from aqueous dispersions employing LiCMC have not been reported previously for lithium-ion batteries. The graphene-platelet composite anode system we have developed possesses high gravimetric capacities (>700 mAh g^{-1}), excellent cycling stability (>100 cycles) and compares favorably to the RGO composite anodes.

2. Experimental

2.1. Materials

MnOOH was obtained from Chemetal Inc., sodium dodecyl sulfate (SDS), $KMnO_4$, graphite flakes, lithium hexafluorophosphate ($LiPF_6$, 99.99%), ethylene carbonate (EC, anhydrous, 99%), dimethyl carbonate anhydrous (DMC, ≥99%), *N*-methyl-2-pyrrolidone (NMP, anhydrous, 99.5%), were purchased from Sigma–Aldrich. xGnP-M-5 graphene platelets (XGM-5) were purchased from xG Sciences (Lansing, MI) and these chemicals were used without further purification. H_2SO_4, H_3PO_4, HCl and ether were purchased from EMD chemicals and used as received. H_2O_2 (30%) was purchased from Fisher Scientific and used as received. KS4 graphite and Super S carbon were purchased from Timcal® (Switzerland), and dried under vacuum at 80 °C overnight. Lithium carboxymethyl cellulose (LiCMC) was prepared from sodium carboxymethyl cellulose using and ion exchange column packed with AG MP-50 resin (Analytical Grade 100–200 Mesh Hydrogen form, Bio-Rad Laboratories Inc.). LiCMC was characterized by NMR and FTIR to insure the carboxymethyl cellulose was intact and by XPS to insure complete ion exchange (see Supporting information).

2.2. Synthesis

2.2.1. Preparation of graphene oxide (GO)

GO was prepared using a modified Hummers method [20]. Graphite flakes (3 g, ~150 μm) and $KMnO_4$ (18 g) were placed in a beaker. A mixture of H_2SO_4/H_3PO_4 (9:1) was added to the solids. The reaction mixture is then heated to 50 °C overnight. The reaction was cooled to room temperature and poured on ice (~400 ml) with H_2O_2 30% (~3 ml). The reaction mixture was sifted through a 300 μm sieve. The filtrate was centrifuged and the supernatant was decanted. The solid was washed in sequence with ~300 ml of water, HCl, 30% and ethanol (2×) with centrifugation and decantation of the supernatant at every step. After the series of washes the solid was suspended in 200 ml of ether and filtered to give a brown-yellow solid.

2.2.2. Preparation of reduced graphene oxide (RGO)

RGO was prepared by annealing GO at 1000 °C for 1 h under H_2/Ar atmosphere with a ramp rate of 5 °C min^{-1}.

2.2.3. Preparation of composite materials

In a typical synthesis MnOOH (254 mg), graphene sample (112 mg) and SDS (40 mg) were suspended in 15 ml of water. The suspension was ultrasonicated for 20 min, then filtered using nanoporous nylon membrane filters (0.2 μm, Whatman), extensively washed with water and dried at 100 °C for 1–2 h. The powder obtained was annealed at 450 °C for 1 h under argon atmosphere with a ramp rate of 5 °C min^{-1}.

2.3. Characterization

Powder X-ray diffraction was carried out using a Bruker AXS D8 diffractometer with a Co Kα source with a divergence angle of 0.3°, a step size of 0.03°, and 1 s per step. The materials were further characterized by scanning electron microscopy (SEM) using a JEOL 840A and by transmission electron microscopy (TEM) using a Philips CM 20 microscope operating at 200 kV. The thermogravimetric analysis (TGA) was performed on the Mn_3O_4/graphene composites using platinum pans in order to quantify their carbon content; a Hi-Res TGA 2950 TA instrument was used. The powder was heated at 10 °C min^{-1} up to 1000 °C in air.

2.3.1. Preparation of the electrodes

The working electrodes were prepared by mixing 80 wt% active material (Mn_3O_4, or graphene, or Mn_3O_4/graphene composite) with, 5 wt% Super S Carbon, 5 wt% graphite E-KS4, and 10 wt% binder. The binder was either LiCMC (2.5 wt% in H_2O) or PVDF (3.0 wt% in NMP). The mixture was mixed with a mixer (Planetary Centrifugal Mixer "THINKY MIXER" ARE-310) at 2000 rpm for 5 min (3×). The slurry was cast onto a high purity copper foil current collector (cleaned using a 2.5% HCl solution) using an automated doctor-blade. The casts were dried in a convection oven at 80 °C overnight. Electrode disks (Ø = 12.5 mm) were punched out pressed at 0.5 metric tons and dried overnight in a vacuum oven at 80 °C. The active materials were tested in half cells using 2325-type coin cells assembled in an Argon-filled box using a metal lithium disk (Ø = 16.5 mm) as a counter and reference electrode. A total of 70 μL of a 1 M solution of $LiPF_6$ in EC:DMC (1:1, v:v) was used as the electrolyte. The electrolyte was spread over a double layer of microporous polypropylene separators (Celgard 3501). Capacity measurements were performed by galvanostatic measurements carried out on a multichannel Arbin battery cycler. The working electrode was first discharged (lithiated) down to 10 mV versus Li/Li^+ at a current density of 75 mA g^{-1} and then charged (delithiated) up to 3.0 V versus Li/Li^+. For the composites, the mass of active material used in the calculation is the mass of the Mn_3O_4 and graphene.

3. Results and discussion

3.1. X-ray diffraction (XRD)

The XRD patterns of both composites, Mn_3O_4/RGO and Mn_3O_4/XGM-5, are shown in Fig. 1. A tetragonal Mn_3O_4 structure (space group $I4_1/amd$) mixed with a graphitic phase was obtained. The Miller indices of both structures have been added to the XRD patterns. The diffraction peaks at 31° and 64° correspond to the graphene phase. The graphene platelets (XGM-5) show a better ordered structure (intense 002 peak) than the synthesized RGO, which is why the Mn_3O_4/XGM-5 pattern looks less noisy.

3.2. Thermogravimetric analysis (TGA)

The composition of the materials was determined using TGA. Fig. 2 shows the thermal decomposition of the composite materials under air. The first two weight losses, occurring between 350 °C and 800 °C, are due to combustion of the carbon in the samples. At the same time a weight gain associated to the oxidation Mn^{II} to Mn^{III} from Mn_3O_4 ($MnO_{1.33}$) to Mn_2O_3 ($MnO_{1.5}$) occurs. However Mn_2O_3 is only stable up to about 900 °C, thus the last weight loss is actually due to the oxygen release that occurs when some Mn^{III} is reduced to Mn^{II} from Mn_2O_3 to re-form Mn_3O_4 [22,23]. The carbon content of the Mn_3O_4/XGM-5 composite is 34.3 wt% while the Mn_3O_4/RGO composite contains 37.7 wt% of carbon.

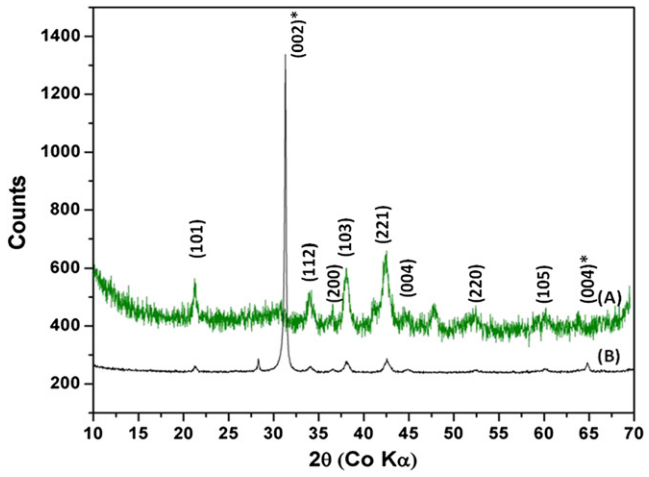

Fig. 1. Powder X-ray diffraction patterns of (A) the Mn_3O_4/RGO composite: Miller indices correspond to Mn_3O_4 (space group: $I4_1/amd$), and (B) the Mn_3O_4/XGM-5 composite: Miller indices correspond to Mn_3O_4 (space group: $I4_1/amd$) and Graphene platelets (see *).

3.3. Scanning electron microscopy (SEM)

The nanostructure and morphological differences between the two composites were characterized by SEM. Fig. 3a and b shows a typical SEM micrograph of the Mn_3O_4/XGM-5 and Mn_3O_4/RGO composite materials, respectively. These images show Mn_3O_4 needle-like particles of approximately 200–450 nm supported by graphene. Fig. 3c and d shows SEM micrographs of the Mn_3O_4/XGM-5 and Mn_3O_4/RGO electrodes. These micrographs are similar to the images of the pristine composite materials with needle-like Mn_3O_4 particles distributed on graphene with the addition of the additives (graphite, Super S carbon, and LiCMC). Based on these images, we see that the composite material leads to a dispersion of graphene platelets and Mn_3O_4 particles in the electrode.

3.4. Electrochemical characterization

The electrochemical performance of the electrode was assessed in a half-cell configuration using lithium metal as a reference and counter electrode. TMOs react with lithium through a reversible conversion reaction, which is very different compared to other electrode materials. While for an intercalation/insertion process, less than 1 electron per metal is typically transferred (e.g. ≈0.5 for cathode materials, 0.6 for $Li_4Ti_5O_{12}$, and 0.17 for graphite), a TMO conversion reaction often transfers 2 electrons per metal (or more), as shown in Eq. (1):

$$Mn_3O_4 + 8Li^+ + 8e^- \rightarrow 3Mn^0 + 4Li_2O \quad (1)$$

During the lithiation step of the conversion reaction Mn_3O_4 is reduced into nanoparticles of manganese and a decomposable matrix of nano-Li_2O is formed. During the delithiation process, nanoparticles of manganese oxide (typically 1–5 nm) are formed; however not necessarily with the same crystalline structure as the starting oxide [1]. Two manganese oxidation paths are reported in the literature. In the first one, Mn^0 is initially oxidized to MnO, and a shoulder that is believed to correspond to the oxidation of MnO to Mn_3O_4 is observed at 2 V on the charge curve [24]. In this case a reversible capacity of 937 mAh g^{-1} is expected. For the second path, the conversion reaction with Mn_3O_4 is believed to occur following the reactions below (see Eqs. (2)–(4)). In this case only reaction (4) has been shown to be reversible. The latter corresponds to a reversible capacity of 703 mAh g^{-1} when considering Mn_3O_4 as a starting material [25].

$$Mn_3O_4 + Li^+ + e^- \rightarrow LiMn_3O_4 \quad (2)$$

$$LiMn_3O_4 + Li^+ + e^- \rightarrow 3MnO + Li_2O \quad (3)$$

$$MnO + 2Li^+ + 2e^- \rightarrow Mn + Li_2O \quad (4)$$

Experimental capacities of the two graphenes were obtained from blank half cells made up of the following: composition 80 wt% graphene, 5 wt% Super S Carbon, 5 wt% graphite KS4 and 10 wt% LiCMC. Stable reversible capacities of 312 mAh g^{-1} and 217 mAh g^{-1} were obtained for XGM-5 and RGO, respectively. The theoretical capacities of the composite materials were calculated from the composition obtained from the TGA measurements as shown below:

$$Mn_3O_4/XGM-5: \ 34.3\ wt\% \times 312\ mAh\,g^{-1} + 65.7\ wt\% \times 937\ mAh\,g^{-1} = 723\ mAh\,g^{-1} \quad (5)$$

$$Mn_3O_4/RGO: \ 37.7\ wt\% \times 217\ mAh\,g^{-1} + 62.3\ wt\% \times 937\ mAh\,g^{-1} = 664\ mAh\,g^{-1} \quad (6)$$

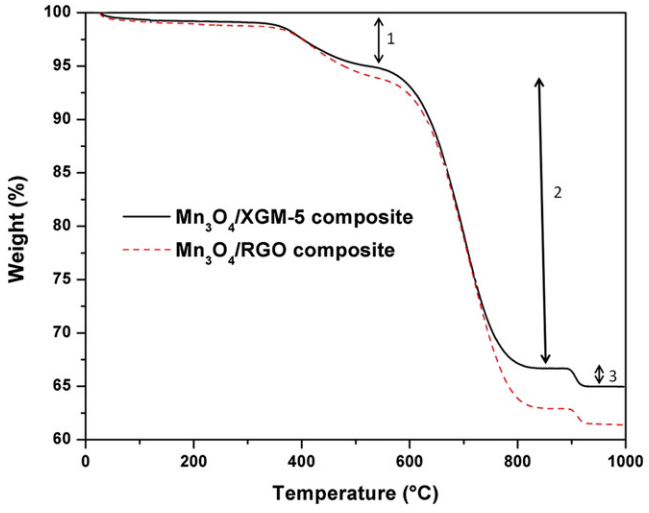

Fig. 2. TGA graph of combustion of Mn_3O_4/graphene composites in air.

3.4.1. Voltage curves

Voltage curves of both composites are shown in Fig. 4. They revealed the expected electrochemical reactions related to processes such as (i) the formation of the solid electrolyte interface (SEI) and (ii) the reduction of Mn^{III} to Mn^{II} (1.25–0.5 V) [26]. The reduction of Mn^{II} to Mn^0 is observed at 0.2 V in the first cycle and at 0.6–0.4 V in subsequent cycles. This is explained by the lithiation becoming easier after the first cycle as the Mn_3O_4 particles are now nanometric in size (lower overpotential). The reversible insertion/deinsertion of Li^+ into XGM-5 and RGO occurs close to 0 V and 0.15 V, respectively. The oxidation of Mn^0 and the decomposition of

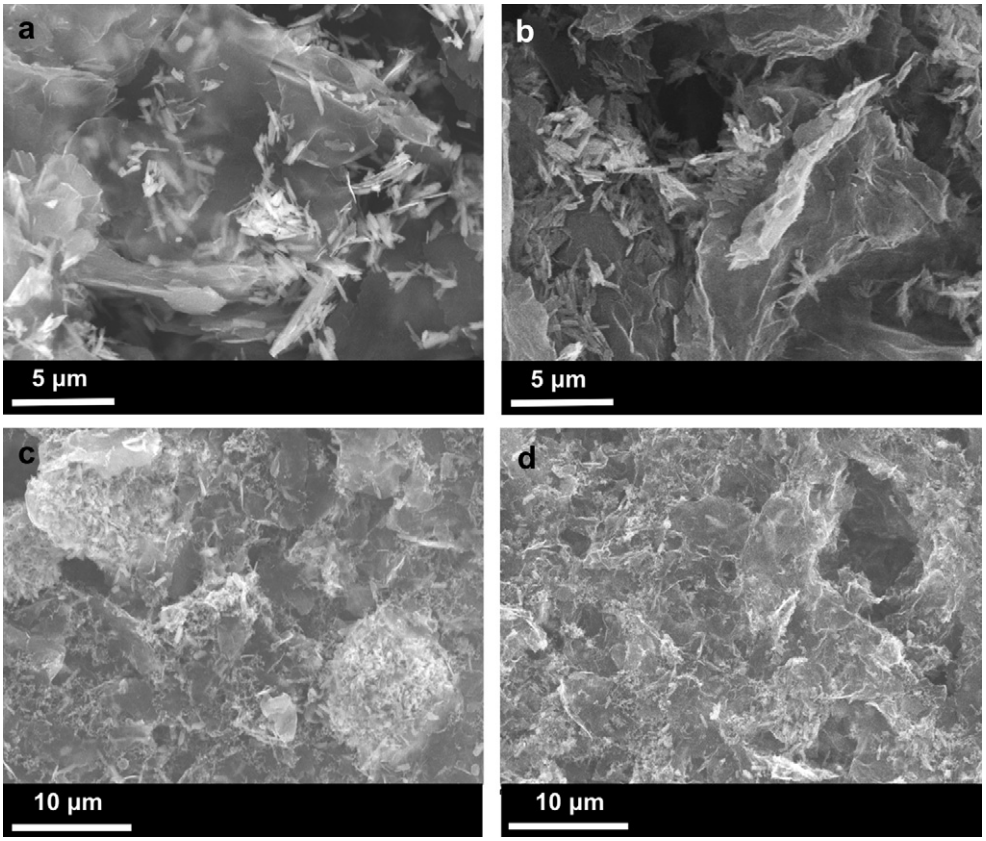

Fig. 3. SEM micrographs of composite materials: (a) Mn_3O_4/XGM-5 (platelet supported Mn_3O_4 needles), and (b) Mn_3O_4/RGO (RGO supported Mn_3O_4 needles). SEM micrographs of composite electrodes made of (c) Mn_3O_4/XGM-5, and (d) Mn_3O_4/RGO.

the nano-Li_2O matrix are observed at 1.3 V. The initial capacity of the Mn_3O_4/XGM-5 composite is 1375 mAh g^{-1} and 1175 mAh g^{-1} for the Mn_3O_4/RGO composite.

Cyclic voltammograms (CVs) of both composites are shown in the Supporting information. They show the expected peaks for the formation of the SEI, the reduction/oxidation of manganese and the insertion/deinsertion of Li^+ in graphene, the results are in accordance with the voltage profiles.

3.4.2. Battery cycling

Fig. 5 shows the battery performance of Mn_3O_4, the graphene platelets (XGM-5), RGO, and both composites. Control experiments in which XGM-5, RGO or Mn_3O_4 are the active anode materials exclusively were also conducted. As previously mentioned, after a large irreversible capacity, the graphenes anodes show low but stable reversible capacities: 312 mAh g^{-1} for XGM-5 and 217 mAh g^{-1} for RGO. As expected, an Mn_3O_4 electrode (without

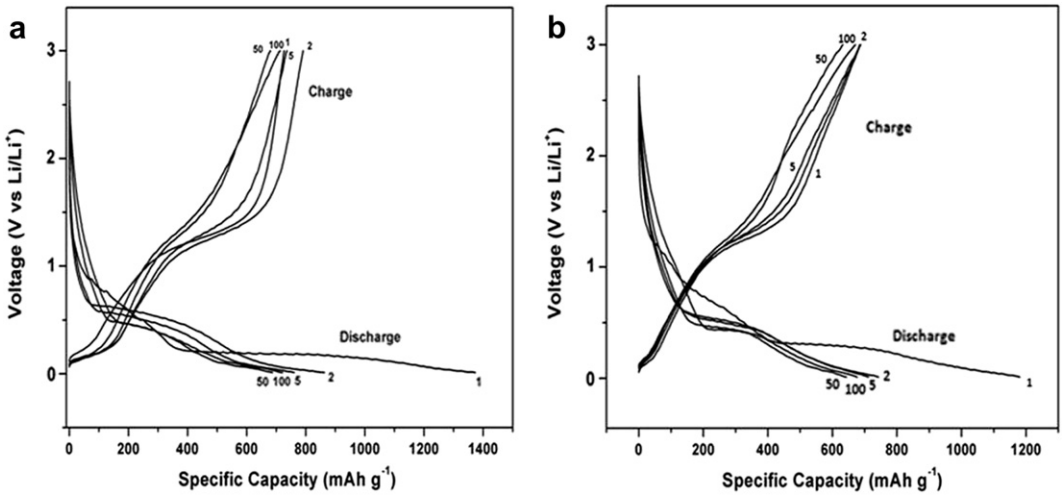

Fig. 4. Voltage profile (discharge/charge) for cycles 1, 2, 5, 50 and 100 of (a) the Mn_3O_4/XGM-5 composite and (b) Mn_3O_4/RGO composite.

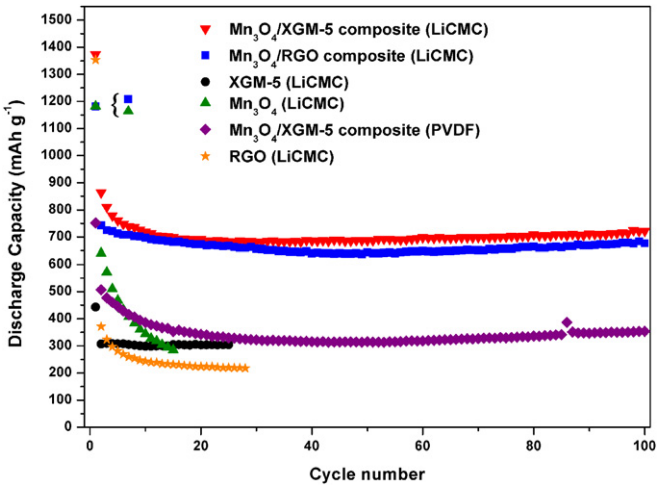

Fig. 5. Cycling performance of Mn_3O_4/graphene composites (0.01–3.0 V), XGM-5 (0.005–2 V) and Mn_3O_4 (0.01–3 V) cycled at 75 mAh g^{-1} with LiCMC or PVDF binder.

graphene) shows a large first discharge capacity of about 1175 mAh g^{-1} that rapidly fades. After only 15 cycles, this electrode shows a capacity of only about 300 mAh g^{-1}, which represents 26% of the first discharge capacity and a continuing downward trend is expected. After initial capacities of 1375 mAh g^{-1} for the Mn_3O_4/XGM-5 composite and 1175 mAh g^{-1} for the Mn_3O_4/RGO composite, both composites showed high and very stable capacities on long term cycling. After 100 cycles, a capacity of approximately 720 mAh g^{-1} was obtained for the Mn_3O_4/XGM-5 composite, which is close to the theoretical capacity (723 mAh g^{-1}) of this composite. The Mn_3O_4/RGO composite showed a reversible capacity of roughly 675 mAh g^{-1} after 100 cycles, which represent the theoretical capacity of this composite. It is interesting to note that the XGM-5 composite performed similarly to the RGO composite, even though the latter had a lower initial capacity. It is important to note that all capacities are based on the total mass of graphene and Mn_3O_4. Beyond the first few cycles, coulombic efficiencies greater than 98% were measured, indicating that graphene/LiCMC composite electrodes enable long term cycling stability with Mn_3O_4 needle-like particles. In our case, the first oxidation path where Mn^0 is oxidized back to Mn_3O_4 probably occurs since the capacities obtained are close to the theoretical capacities (when using 937 mAh g^{-1} as the theoretical capacity for Mn_3O_4).

A further comparison using PVDF as binder and *N*-methyl pyrrolidone (NMP) as the casting solvent, which is a typical electrode processing method for commercial lithium-ion batteries, was performed with both composites. Interestingly, the capacity of these anodes was <400 mAh g^{-1} after only 10 cycles (see Fig. 5). This result further exemplifies the important role LiCMC plays in largely mitigating the effect of volume changes during cycling. The superior capacity retention with LiCMC is believed to be due to the formation of bonds between the carboxyl groups of the binder and hydroxyl groups present at the surface of the metal oxide, as observed with silicon and NaCMC based anodes [27,28]. In addition, NaCMC extended conformation in solution facilitates a networking process of the conductive additive [29]. In the case of silicon, it has been shown that stronger mechanical contacts within the composite electrode in addition to the CMC bridging of the Si and carbon black particles can be obtained by buffering the aqueous solution which promotes covalent bonding [30]. An additional explanation to the better performance of CMCs is its better ability to cover the particles compared to PVDF which results in stronger interparticle bonding in addition to the formation of a better SEI layer [31,32].

4. Conclusion

In summary, we have successfully prepared high capacity composite anodes with long cycle life comprising Mn_3O_4, graphene, and LiCMC. The Mn_3O_4/graphene-platelets composite showed better performance than the Mn_3O_4/RGO composite (720 mAh g^{-1} versus 675 mAh g^{-1}), thus demonstrating that relatively thicker graphene platelets can effectively support TMO particles in lithium-ion battery composite anodes. Furthermore, the electrodes were cast from aqueous dispersions in which LiCMC was used as a binder, enabling a manufacturing process void of volatile organic compound (VOC) emissions. LiCMC formulations further provided superior performance compared to PVDF, presumably due to enhanced nano-architecture and interface interactions with the active materials, resulting in near theoretical capacities to be achieved after 100 cycles. Our work presents the first instance in which the virtues of LiCMC have been extended to graphene based anode systems as well as the use of graphene platelets in LIB anodes.

Acknowledgements

This work was supported by Natural Resources Canada's Office of Energy Research and Development (Electric Mobility Program of Energy Research and Development: PERD project number C51.003).

Appendix A. Supplementary data

Supplementary data related to this article can be found online at doi:10.1016/j.jpowsour.2012.03.055

References

[1] P. Poizot, S. Laruelle, S. Grugeon, L. Dupont, J.M. Tarascon, Nature 407 (2000) 496–499.
[2] M.V. Reddy, T. Yu, C.H. Sow, Z.X. Shen, C.T. Lim, G.V. Subba-Rao, B.V.R. Chowdari, Adv. Funct. Mater. 17 (2007) 2792–2799.
[3] Y. Li, B. Tan, Y. Wu, Nano Lett. 8 (2008) 265–270.
[4] Z.-M. Cui, L.-Y. Jiang, W.-G. Song, Y.-G. Guo, Chem. Mater. 21 (2009) 1162–1166.
[5] K. Zhong, X. Xia, B. Zhang, H. Li, Z. Wang, L. Chen, J. Power Sources 195 (2010) 3300–3308.
[6] F.M. Courtel, Y. Abu-Lebdeh, I.J. Davidson, Electroch. Acta. 71 (2012) 123–127.
[7] B. Varghese, M.V. Reddy, Z. Yanwu, C.S. Lit, T.C. Hoong, G.V. Subba Rao, B.V.R. Chowdari, A.T.S. Wee, C.T. Lim, C.-H. Sow, Chem. Mater. 20 (2008) 3360–3367.
[8] H. Dhaouadi, A. Madani, F. Touati, Mater. Lett. 64 (2010) 2395–2398.
[9] Y. Zhu, M.D. Stoller, W. Cai, A. Velamakanni, R.D. Piner, D. Chen, R.S. Ruoff, ACS Nano 4 (2010) 1227–1233.
[10] G. Zhou, D.-W. Wang, F. Li, L. Zhang, N. Li, Z.-S. Wu, L. Wen, G.Q. Lu, H.-M. Cheng, Chem. Mater. 22 (2010) 5306–5313.
[11] H. Wang, L.-F. Cui, Y. Yang, H. Sanchez Casalongue, J.T. Robinson, Y. Liang, Y. Cui, H. Dai, J. Am. Chem. Soc. 132 (2010) 13,978–13,980.
[12] S. Yang, X. Feng, S. Ivanovici, K. Müllen, Angew. Chem. Int. Ed. 49 (2010) 8408–8411.
[13] G. Wang, T. Liu, X. Xie, Z. Ren, J. Bai, H. Wang, Mater. Chem. Phys. 128 (2011) 336–340.
[14] X. Zhu, Y. Zhu, S. Murali, M.D. Stoller, R.S. Ruoff, ACS Nano 5 (2011) 3333–3338.
[15] Z.-S. Wu, W. Ren, L. Wen, L. Gao, J. Zhao, Z. Chen, G. Zhou, F. Li, H.-M. Cheng, ACS Nano 4 (2010) 3187–3194.
[16] S.Q. Chen, Y. Wang, J. Mater. Chem. 20 (2010) 9735–9739.
[17] Y.-S. He, D.-W. Bai, X. Yang, J. Chen, X.-Z. Liao, Z.-F. Ma, Electrochem. Commun. 12 (2010) 570–573.
[18] W.S. Hummers, R.E. Offeman, J. Am. Chem. Soc. 80 (1958) 1339.
[19] N.I. Kovtyukhova, P.J. Ollivier, B.R. Martin, T.E. Mallouk, S.A. Chizhik, E.V. Buzaneva, A.D. Gorchinskiy, Chem. Mater. 11 (1999) 771–778.
[20] D.C. Marcano, D.V. Kosynkin, J.M. Berlin, A. Sinitskii, Z. Sun, A. Slesarev, L.B. Alemany, W. Lu, J.M. Tour, ACS Nano 4 (2010) 4806–4814.
[21] F.M. Courtel, S. Niketic, D. Duguay, Y. Abu-Lebdeh, I.J. Davidson, J. Power Sources 196 (2011) 2128–2134.
[22] V. Berbenni, A. Marini, Mater. Res. Bull. 38 (2003) 1859–1866.

[23] S. Fritsch, J. Sarrias, A. Rousset, G.U. Kulkarni, Mater. Res. Bull. 33 (1998) 1185–1194.
[24] J. Gao, M.A. Lowe, H.D. Abruña, Chem. Mater. 23 (2011) 3223–3227.
[25] X. Fang, X. Lu, X. Guo, Y. Mao, Y.-S. Hu, J. Wang, Z. Wang, F. Wu, H. Liu, L. Chen, Electrochem. Commun. 12 (2010) 1520–1523.
[26] K. Kanamura, S. Shiraishi, H. Tamura, Z.-I. Takehara, J. Electrochem. Soc. 141 (1994) 2379–2385.
[27] N.S. Hochgatterer, M.R. Schweiger, S. Koller, P.R. Raimann, T. Wohrle, C. Wurm, M. Winter, Electrochem. Solid-State Lett. 11 (2008) A76–A80.
[28] J. Li, H.M. Dahn, L.J. Krause, D.-B. Le, J.R. Dahn, J. Electrochem. Soc. 155 (2008) A812–A816.
[29] B. Lestriez, S. Bahri, I. Sandu, L. Roué, D. Guyomard, Electrochem. Commun. 7 (2007) 2801–2806.
[30] D. Mazouzi, B. Lestriez, L. Roue, D. Guyomard, Electrochem. Solid-State Lett. 12 (2009) A215–A218.
[31] L. El Ouatani, R. Dedryvère, J.-B. Ledeuil, C. Siret, P. Biensan, J. Desbrières, D. Gonbeau, J. Power Sources 189 (2009) 72–80.
[32] V. Sivasankaran, C. Marino, M. Chamas, P. Soudan, D. Guyomard, J.C. Jumas, P.E. Lippens, L. Monconduit, B. Lestriez, J. Mater. Chem. 21 (2011) 5076–5082.